

Optimal Control for Minimizing Power Consumption During Holding Patterns for Airborne Wind Energy Pumping System

G. Licitra¹, S. Sieberling¹, S. Engelen¹, P. Williams¹, R. Ruiterkamp¹ and M. Diehl².

Abstract—Airborne Wind Energy (AWE) concerns systems capable harvesting energy from the wind, offering an efficient alternative to traditional wind turbines by flying crosswind with a tethered airfoil. Such concepts involve a system more difficult to control than conventional wind turbines. These systems generally cannot be operated efficiently in very low wind conditions, necessitating intervention by launching and landing. In contrast to this approach, this paper proposes to continue flying holding patterns which minimize power consumption. Efficient holding patterns are determined by solving an optimal control problem. The model is specified as a set of differential algebraic equations and an approximation of the tether drag is taken into account. Finally, an evaluation in terms of energy is performed by means of statistical approach.

Keywords: Airborne Wind Energy, optimal control, differential algebraic equation, tether drag, low wind conditions.

I. INTRODUCTION

In a world of continuing industrialization the demand for energy is growing. Energy mainly comes from polluting processes causing atmospheric changes. Renewable energy systems such as solar systems and wind turbines have been designed in order to reduce the effects of climate changes. However there are physical constraints related to renewable systems, e.g. it is not possible to arbitrarily increase the size of conventional wind turbines. As an alternative, new technologies are developed that aim to remove all the structural elements of a conventional wind turbine, consequently allowing green power at a competitive cost compared to non-renewable sources. These technologies are known as Airborne Wind Energy Systems (AWES). A wide variety of concepts in the field of AWES can be found in literature [1], although according to [4] two main branches can be distinguished. *Drag mode AWES* generate power using on board turbines, relaying power to the ground via a conductive tether. A drag mode AWES is being developed by Makani Power [3]. *Lift mode* or *Pumping mode AWES* produce power by performing periodical variation of tether length and

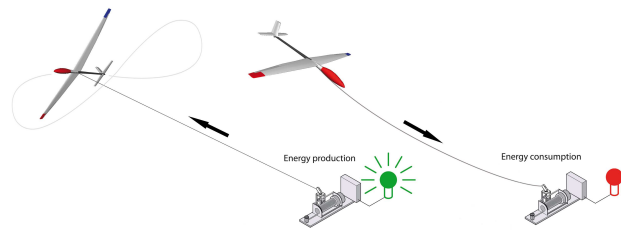


Fig. 1. Example of a pumping cycle with a reel-in and reel-out phase

tether tension. A *pumping mode* AWES is being developed by Ampyx Power [2] which they call a "PowerPlane". Fig. 1 shows an artist impression of the two main phases of a *pumping mode* AWES. In a *pumping* system, the generator is located on the ground. Power generation occurs during a so called "reel-out phase", where the tether tension is used to rotate a drum, driving an electric generator. A reel-in phase is required due to finite tether length. By changing the flight pattern in such a way that less lifting force is produced, the tether can be wound with a significant lower energy investment than what was gained in the power production phase. For low wind conditions the amount of energy consumed during reel-in can exceed the amount of energy generated during reel-out. In this case one might prefer to land until favorable wind conditions occur. Landing and launching a *pumping mode* AWES requires sophisticated and expensive startup methodology. One possible launch and landing mechanism uses a rotating arm around a central axis [23] but alternative launch mechanisms such as a pneumatic catapult are also investigated by different AWES developers. Moreover, the tether plays an important role in the behavior of AWES as described in [10]. Circular optimal trajectories were computed successfully using a full six degree of freedom aircraft model [12], but no tether drag was taken into account.

In this paper, holding patterns for minimizing power consumption during low wind condition are computed by solving an optimal control problem. The solution is analyzed by comparing the cost of the energy required to maintain the holding patterns against the cost of implementing a mechanical launch and land platform. The chapters are organized as follows. Section II presents a model for *pumping mode* AWES based on a multi-body approach which include a full six degree of freedom aircraft model and an approximation of tether drag. The parameters of the system are based on the second generation prototype developed by Ampyx Power. Section III presents the formulation of the optimal control

*The work leading to these results/this invention has received funding from the People Programme (Marie Curie Actions) of the European Unions Seventh Framework Programme (FP7/2007-2013) under REA grant agreement no 607957 (TEMPO).

¹ Ampyx Power B.V., Lulofsstraat 55, 2521 AL Den Haag, The Netherlands.

G.Licitra@ampyxpower.com
S.Sieberling@ampyxpower.com
S.Engelen@ampyxpower.com
P.Williams@ampyxpower.com
R.Ruiterkamp@ampyxpower.com

² Institute of Microsystems Engineering (IMTEK) University of Freiburg, 79110 Freiburg Im Breisgau, Germany
moritz.diehl@imtek.uni-freiburg.de

problem, specifying the physical constraints and boundary conditions for periodic trajectories. Section IV shows the computed results: a first result is related to the tether drag contribution; afterwards the typical trend of optimal patterns is shown for low wind conditions; finally an estimation of energy balance over one year is evaluated in the case of continuous operation of the *Pumping mode* AWES.

II. MODELIZATION OF THE PHYSICAL PLANT

A. Modeling of the *Pumping mode* AWES

Pumping mode AWES is modeled using a multi-body approach. It is straightforward to see the generation device on the ground and the aircraft as two distinct bodies, which interact through the tether. For each body, an orthonormal right-hand reference frame is defined. Let \mathbf{E} the reference frame with origin coinciding to the generator and \bar{E}_z concordant to the gravitational acceleration vector g . It is assumed that the wind speed increases logarithmically as function of the altitude h [5], with direction towards to \bar{E}_x .

$$w(h) = w(h_0) \frac{\ln(\frac{h}{h_r})}{\ln(\frac{h_0}{h_r})} \quad (1)$$

where $w(h_0)$ is the wind velocity at altitude h_0 and h_r the roughness length (details can be found in [24]). In the same way, let \mathbf{e} be the conventional body reference frame attached to the aircraft with its origin coinciding to the center of gravity (CG) of the aircraft, where the basis vector \bar{e}_x spans the wing longitudinal axis, pointing in the forward direction and is aligned with the wing chord and the basis vector \bar{e}_z spans the vertical axis, pointing in the downward direction.

According to [14], the tether is approximated as a rigid link of length l time-varying, while the position of the aircraft CG in the reference frame \mathbf{E} is given by the coordinate vector $\bar{r} = [x, y, z]^T$, where x, y, z are the Cartesian coordinates. Due to the use of non-minimal coordinates, an additional constraint equation is required to recover the tether tension from the inelastic constraint. Thus, with such formulation \bar{r} is constrained to evolve on the manifold described by the single constraint

$$C = \frac{1}{2} (\bar{r}^T \bar{r} - l^2) = 0 \quad (2)$$

The assumption of rigid link requires that the tether always has to be under tension, although in practice it could be realistic only during reel-out phase. Fig. 2 summarizes the axis definition. If the tether is attached at the CG of the aircraft, the dynamic model can be written as follow

$$\begin{bmatrix} (m_a + \frac{1}{3}m_T)I_3 & 0 & \bar{r}/l \\ 0 & \bar{J} & 0 \\ \bar{r}^T & 0 & 0 \end{bmatrix} \begin{bmatrix} \ddot{\bar{r}} \\ \ddot{\bar{\omega}} \\ F_T \end{bmatrix} = \begin{bmatrix} \bar{F} + (m_a + \frac{1}{3}m_T)g\bar{1}_z \\ \bar{M} - \bar{\omega} \times \bar{J}\bar{\omega} \\ -\dot{\bar{r}}^T \dot{\bar{r}} + \dot{l}^2 + l\ddot{l} \end{bmatrix} \quad (3)$$

where \bar{I}_3 the identity matrix, $\bar{1}_z = [0, 0, 1]^T$ is the unit vector in the z -direction, m_a, m_T are respectively aircraft and tether

mass, \bar{J} the inertia matrix, $\bar{\omega} = [p, q, r]^T$ the vector of angular velocity in wing reference \mathbf{e} . The tension force F_T appears in the aircraft dynamics, and is resolved in (3) by adding the second derivative of (2) as a coupled equation. This results in a set of differential algebraic equations [14], while \bar{F} and \bar{M} are respectively the aerodynamic forces and torques of the aircraft, with an approximation of tether drag included (details in Appendix A). As far as it regards the rotational kinematic of the aircraft is given by

$$\dot{\mathbf{R}} = \mathbf{R} \Omega \quad (4)$$

with $\mathbf{R} = [\bar{e}_x, \bar{e}_y, \bar{e}_z]$ and Ω the skew matrix of $\bar{\omega}$.

During the reel-out phase, the generator is driven by the tether tension F_T , thus the mechanical power will be the latter force, times the unrolling speed of the tether

$$P_{mech} = F_T \dot{l} \quad (5)$$

It is straightforward to retrieve the angular magnitudes related to the winch

$$\omega_{winch} = \frac{\dot{l}}{r_{winch}} \quad (6)$$

$$\tau_{winch} = F_T r_{winch} \quad (7)$$

where ω_{winch} and r_{winch} are respectively the angular velocity and radius of the winch, with τ_{winch} its torque (see Fig. 3). The generation device, as well as the airplane are subject to constraints due to physical limits. These can be taken into account by means of an optimal control problem.

B. Modeling of tether drag

The main difference between a conventional aircraft and tethered aircraft, is the presence of a tether which induces additional drag, moments (if the tether is not placed in CG of the aircraft) and weight. The latter was already taken into account in (3), while the tether drag has to be modeled properly since it gives a substantial contribution to the overall system. In this paper the tether drag is derived for low wind conditions, assuming the cable velocity V_t is a linear function

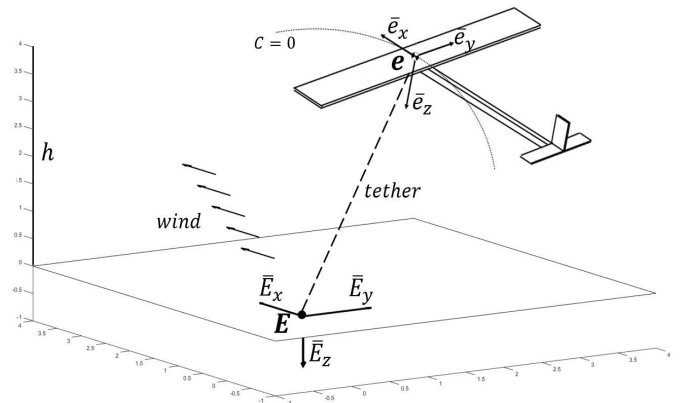


Fig. 2. Schematic of references frame \mathbf{E} and \mathbf{e} , manifold and wind direction

of both the length l and of the aircraft velocity V_a , the latter with direction always orthogonal to the cable, i.e.

$$V_t \approx \frac{s}{l} V_a \quad s \in [0, l] \quad (8)$$

where s is a spatial coordinate along the cable of length l (Fig. 4). The drag force for an elemental portion ds of the cable is

$$D_s = \frac{1}{2} \rho V_t^2 C_{D_N} d \, ds \quad (9)$$

where ρ air density, C_{D_N} and d are drag coefficient and thickness of the tether. The moment due to drag, taken around the winch position, is

$$M_{D_s} = \frac{1}{2} \rho V_t^2 C_{D_N} d \, ds \, s \quad (10)$$

Thus, the total moment due to drag is give by the integral

$$M_{D_t} = \int_0^l \frac{1}{2} \rho \left(\frac{s}{l} V_a \right)^2 C_{D_N} d \, ds \, s = \frac{1}{8} \rho V_a^2 C_{D_N} d l^2 \quad (11)$$

with equivalent drag force on the aircraft [9]

$$D_t = \frac{1}{8} \rho V_a^2 C_{D_N} d l \quad (12)$$

In aerospace aerodynamic the convention is to normalize forces by dividing by dynamic pressure times the wing surface area S , i.e. $\frac{1}{2} \rho V_a^2 S$. Hence, the drag coefficient of the tether normalized with respect to the aircraft is [11]

$$C_{D_t} = \frac{C_{D_N} d}{4S} l \quad (13)$$

III. FORMULATION OF THE OPTIMAL CONTROL PROBLEM

The prevalent aim of any AWE system is to maximize the average power output. The latter, can be written as an integral over the pattern along the time horizon T . In our case, since the harvested energy comes from the tether tension and the model of the winch does not include any electrical part, the mechanical power given by (14) will be maximized

$$P_{AV} = \frac{1}{T} \int_0^T P_{mech}(t) dt = \frac{1}{T} \int_0^T F_T(t) l(t) dt \quad (14)$$

Moreover a quantity often penalized in an optimization problem is the integral of squared control action $\mathbf{u}(t)$ both

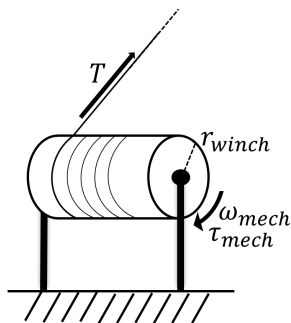


Fig. 3. Sketch of the winch during reel-out phase

for discouraging aggressive maneuvers and to keep the optimization problem well posed, improving convergence [12], [22]. In this paper we also choose to penalize the side slip angle β (details in appendix A) in order to avoid undesired side forces and additional drag on the airplane. Thus, the objective function can be written as

$$J = \frac{1}{T} \int_0^T \|\mathbf{u}(t)\|_{\Sigma_u^{-1}}^2 + \sigma^{-1} \beta^2(t) - F_T(t) l(t) dt \quad (15)$$

where Σ_u^{-1} and σ^{-1} are definite positive weighting matrices with proper sizes.

The model explained in section II can be expressed as a set of implicit differential-algebraic equation (DAE):

$$0 = \mathbf{f}(\dot{\mathbf{x}}, \mathbf{x}, \mathbf{z}, \mathbf{u}, \mathbf{p}, t) \quad (16)$$

with state $\mathbf{x} = [\bar{r}, \dot{\bar{r}}, \bar{e}_x, \bar{e}_y, \bar{e}_z, \bar{\omega}, l, \dot{l}, \phi_a, \phi_e, \phi_r]^T \in \mathfrak{R}^{24}$, where ϕ_a, ϕ_e, ϕ_r stand respectively for aileron, elevator and rudder deflection. The input vector is defined by $\mathbf{u} = [\ddot{l}, \dot{\phi}_a, \dot{\phi}_e, \dot{\phi}_r]^T \in \mathfrak{R}^4$, the algebraic variable $\mathbf{z} = F_T \in \mathfrak{R}$, while the vector \mathbf{p} gathers all the parameters of the *Pumping mode* AWES and t is time. The control actuators are incorporated into the state equations so that practical limits can be applied to the actuator rates in the problem formulation. The minimization of the rates in the cost function also helps to generate smoother output trajectories. The formulation of our optimal control problem (OCP) in continuous time can be stated as follows

$$\begin{aligned} & \underset{\mathbf{x}, \mathbf{z}, \mathbf{u}, T}{\text{minimize}} && J(\mathbf{x}, \mathbf{u}, \mathbf{z}, \mathbf{p}, t, T) \\ & \text{subject to} && \mathbf{f}(\dot{\mathbf{x}}, \mathbf{x}, \mathbf{z}, \mathbf{u}, \mathbf{p}, t) = 0, t \in [0, T] \\ & && \mathbf{h}(\mathbf{x}, \mathbf{z}, \mathbf{u}, \mathbf{p}, t) \leq 0, t \in [0, T] \\ & && T_{min} < T < T_{max} \\ & && \mathbf{c}(\mathbf{x}_0, \mathbf{x}_T) = 0 \end{aligned} \quad (17)$$

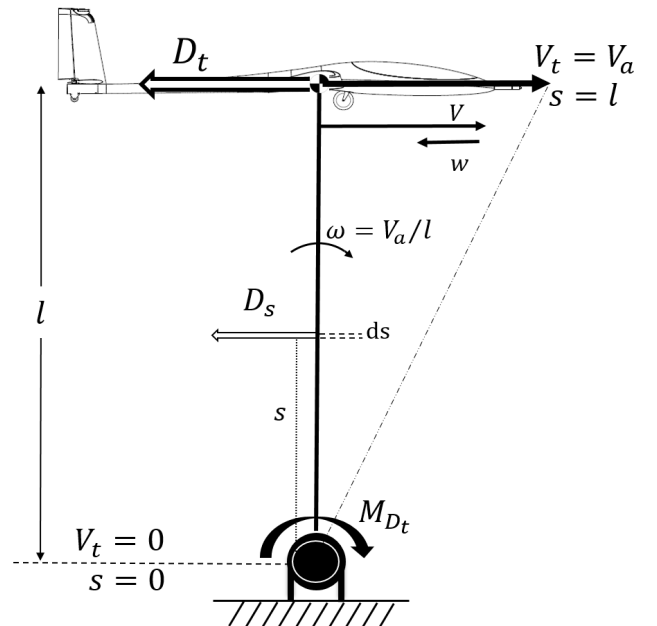


Fig. 4. Representation of tether drag

where \mathbf{h} and \mathbf{c} are respectively the path and boundary constraint functions. OCPs in continuous time domain as (15) can be first approximated by a finite dimensional nonlinear program (NLP) and then solved through a general-purpose NLP solver [18]. For long integration times, a correction of the numerical drift may be needed both for the orthonormality of \mathbf{R} and for the dynamics relative to (2) (details in [14], [15], [17]). However, this is not required in the framework of Model Predictive Control [25]. Finally, Since the NLP is in general non-convex due to the nonlinear dynamics constraints, the NLP solver will only find a local solution. The latter depends greatly on the initial guess, and globalization strategies need to be employed in order to retrieve a good initial guess [26]. In this work the homotopy strategy is used (details in [15]).

A. Characterization of path constraints

The path constraints are mainly related to the physical limitations of the *Pumping mode* AWES and they can be summarized as follow (details in appendix A):

- True airspeed of the aircraft as well as the altitude need lower bounds for safety issues.
- Angle of attack α is bound to be less than the value at which stall is expected.
- Side-slip angle is limited between $\beta_{min} \leq \beta \leq \beta_{max}$ in order to bound side forces.
- Control surfaces ϕ_a, ϕ_e and ϕ_r of the aircraft are subject to limitations both in angles and speeds, related to the installed servos.
- Mechanical torque τ_{winch} is upper limited since it is strictly related to the tether tension F_T , and the latter can lead both to unacceptable mechanical stress of the aircraft and tether severance.
- Constraints related to the tether l, \dot{l}, \ddot{l} , depend on the intrinsic characteristics of the generation device.
- Constraint $F_T > 0$ is required to keep the tether under tension.

B. Characterization of boundary conditions

Boundary constraints are defined a function of both the type of formulation employed in section II and for the requirement of periodicity related to the NLP solution. They can be summed as follows:

- Since the model equations use non-minimal coordinates (i.e., there are more generalized coordinates than degrees of freedom), the algebraic constraint (2) must be enforced as initial condition, as well as its respective derivative [14]

$$\bar{r}_0^T \bar{r}_0 - l_0^2 = 0 \quad (18)$$

$$\bar{r}_0^T \dot{\bar{r}}_0 - l_0 \dot{l}_0 = 0 \quad (19)$$

Similarly, the initial rotation matrix \mathbf{R} must be orthonormal i.e.

$$0 = \mathbf{R}_0^T \mathbf{R}_0 - \mathbf{I} \quad (20)$$

- The periodicity condition is usually enforced simply by $x_0 = x_T$, however, because of the non-minimal coordinates, the latter condition would produce an overconstrained NLP which will cause problems in the NLP solution. Thus, the periodic condition will be [12]

$$\begin{bmatrix} l_0 \\ y_0 \\ z_0 \\ \dot{l}_0 \\ \dot{y}_0 \\ \dot{z}_0 \\ \ddot{l}_0 \\ \ddot{\omega}_0 \\ \phi_0 \end{bmatrix} = \begin{bmatrix} l_T \\ y_T \\ z_T \\ \dot{l}_T \\ \dot{y}_T \\ \dot{z}_T \\ \ddot{l}_T \\ \ddot{\omega}_T \\ \phi_T \end{bmatrix} \quad (21)$$

as well as the three upper off-diagonal components of

$$\mathbf{R}_0^T \mathbf{R}_T = \mathbf{I} \quad (22)$$

where the subscripts refer to the initial and final time.

Hence, the equations (18),(19),(20),(21),(22) represent the boundary condition $\mathbf{c}(\mathbf{x}_0, \mathbf{x}_T) = 0$ of the OCP in (15).

IV. EXPERIMENTAL RESULTS

The OCP is solved by a direct collocation technique using degree 4 interpolating polynomials with Radau polynomial roots as collocation points [12]. The optimization problem was built using *CasADi*, a symbolic framework for algorithmic differentiation and numeric optimization [6] in the Python environment (version 2.7.10) and using *RAWESOME Airborne Wind Energy Simulation, Optimization and Modeling Environment* [7]. The NLP solver employed was *IPOPT*, a software package for large-scale nonlinear optimization [8]. The model parameters come from the second generation of prototype designed by Ampyx Power B.V. [27], Fig. 5. shows both the generator located on the ground and the powerplane.

A. Effect of tether drag on the Pumping mode AWES

Fig. 6,7 show the drastic effect that tether drag has on the system performance. In the absence of tether drag, the PowerPlane exploits the total available tether length in order to reach high altitudes where the wind is more consistent. The system works in boundary regions, using maximum tether speed and torque in order to harvest as much energy as possible and a single reel-in phase occurs for each loop. The average mechanical power produced at each loop is equal to 13.15 kW. Once the tether drag is taken into account, it is no longer optimal to fly at higher altitudes and longer tether lengths due to the losses incurred from the total drag. The reel-in (consumption) phase is completed as quickly as possible but twice per loop at the corners of the pattern. In these regions the power production is least efficient due to the reduction in cross-wind motion. Average mechanical power for this case is downsized at 9.67 kW per loop. Fig. 8 shows the significant contribution (linear) provided by the tether over the total drag.



Fig. 5. Generator and Powerplane owned by Ampyx Power B.V.

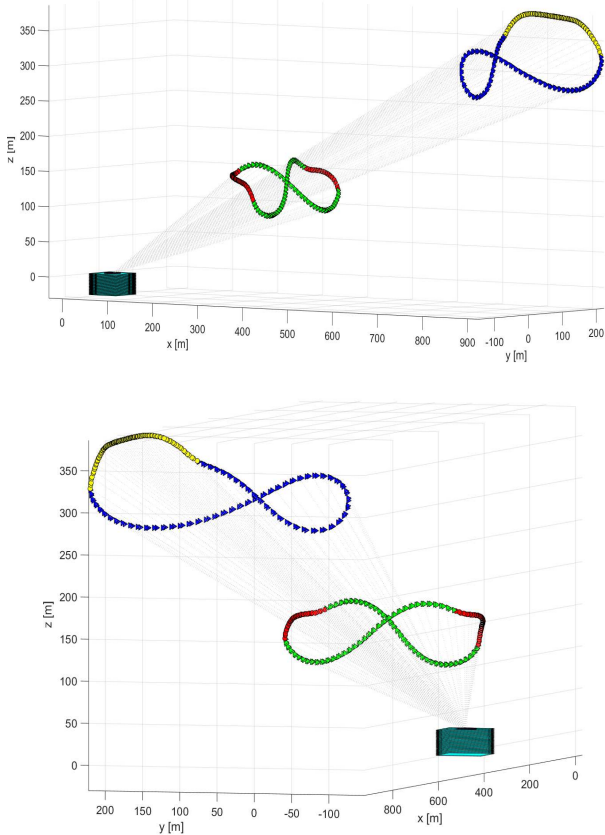


Fig. 6. Comparison of patterns with and without tether drag in 3D. wind speed $w(h_0) = 10 \frac{m}{s}$. Blue arrow-shaped line for reel-out (production) phase and yellow arrow-shaped line for reel-in (consumption) phase for case with tether drag neglected. Green arrow-shaped line for reel-out phase and red arrow-shaped line for reel-in phase for case with tether drag included.

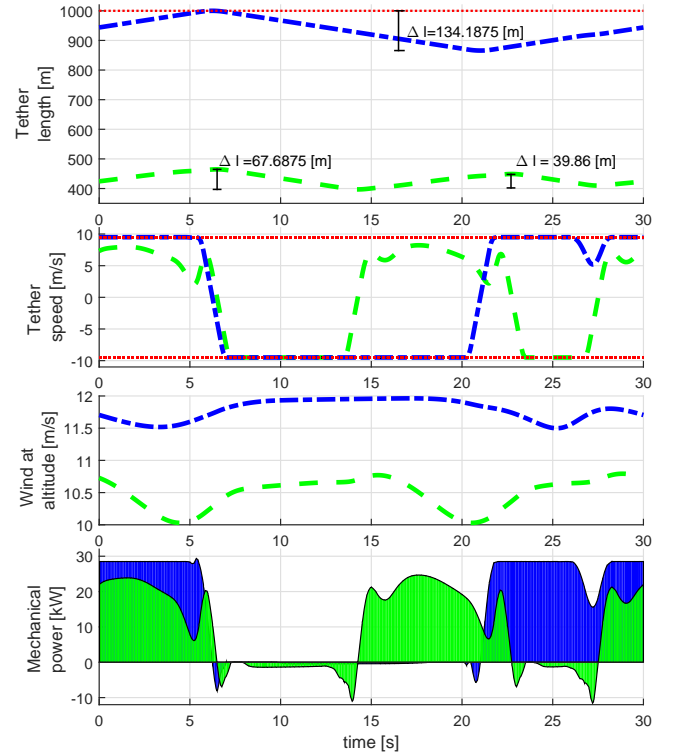


Fig. 7. Comparison related to the tether drag effect: green dashed line for the case with tether drag, blue dash-dot line for case with tether drag neglected, dotted red line for constraints

B. Optimal holding patterns for low wind conditions

For this simulation, optimal holding patterns which approach zero wind speed are computed. The range of wind speed chosen is between 0 and 3 m/s with a step size of 0.5 m/s at altitude $h_0 = 100$ m. The minimum altitude allowed was set at $h_{min} = 100$ m. Fig. 9 shows that with decreasing wind speed, the trajectories get closer to the generator, reducing at the same time their inclinations. As in the previous case, the reel-in phase occurs in the corners for all cases. In low wind conditions, the winch is used to insert kinetic energy into the system. The speed of the aircraft increases when the tension on the tether is increased by the winch. The gained speed is then converted into potential energy and it is repeated cyclically. For this simulation, the system starts to produce power from $w(h_0) \approx 2.5$ m/s.

C. Statistical analysis for power production related to holding patterns

It is possible to make a trade-off between continuous flying without landing during disadvantageous wind conditions in terms of cost of a complex landing device and power consumed during holding patterns over a year. The analysis could be done using a statistical approach employed for wind turbines. The power available from a generic AWE system can be shown using power curves vs wind, while the probability of a wind speed that occurs, between a fixed range of wind at desired location and height, can be summarized by means of Weibull probability density function. Fig.

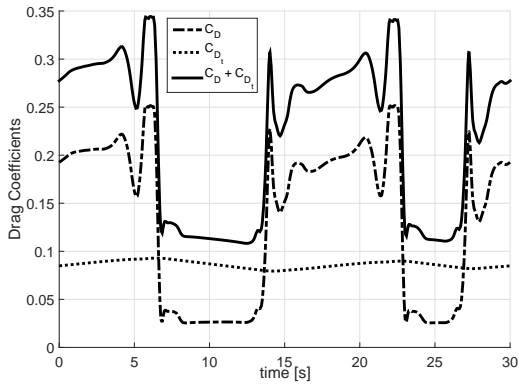


Fig. 8. Tether drag effect over total drag: C_D in dash-dot line related to the airplane drag coefficient; C_{D_t} in dotted line for the tether drag coefficient; $C_D + C_{D_t}$ in solid line for the total drag coefficient.

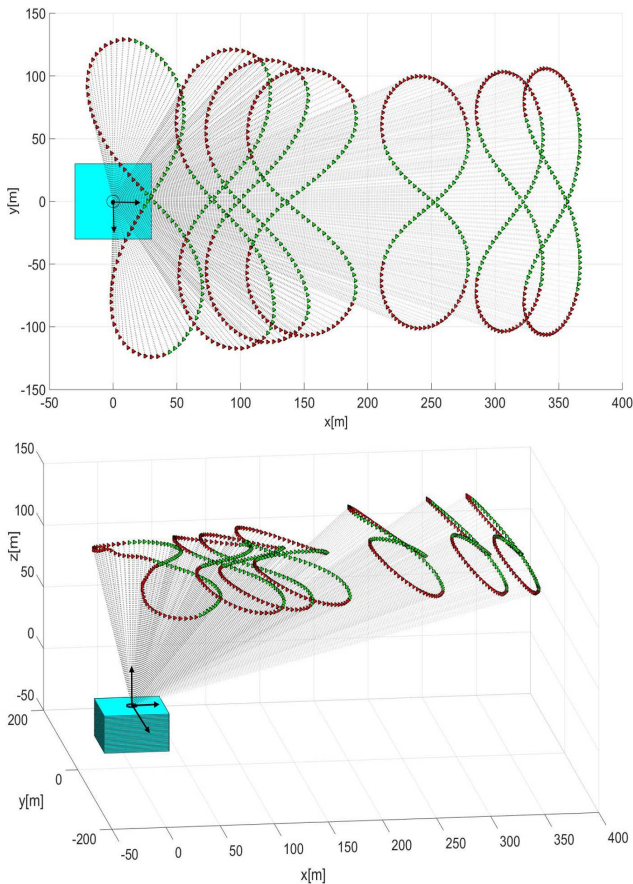


Fig. 9. Optimal holding patterns during low wind conditions: red arrow-shaped line for reel-in (consumption) phase; green arrow-shaped line for reel-out (production) phase.

10 shows the power curve related to the specific *Pumping mode* AWES, the wind class 2 wind distribution [28] and the average wind Energy \bar{E}_w . The latter can be computed from average mechanical wind power \bar{P}_w by the integration of the product between power curve times the probability density function of wind speed. Moreover, it is assumed that the system must land for wind speed over 22.5 m/s for safety issues. Such analysis reveals that the relative cost, i.e. the ratio between the energy consumption to keep the system aloft (using optimal holding patterns) and the total energy harvested by the system is 0.5%. The total energy used is 274 kWh while the total energy harvested is equal to 52.27 MWh, that is approximately 52 MWh of energy produced by a small *Pumping mode* AWES in one year. Finally, it is interesting to evaluate the system in terms of capacity factor. This can be expressed by the ratio of actual power output over a year and the potential maximum output if it were possible for the AWE system to operate at full capacity continuously over one year. For such system, the capacity factor is equal to 52.54 %.

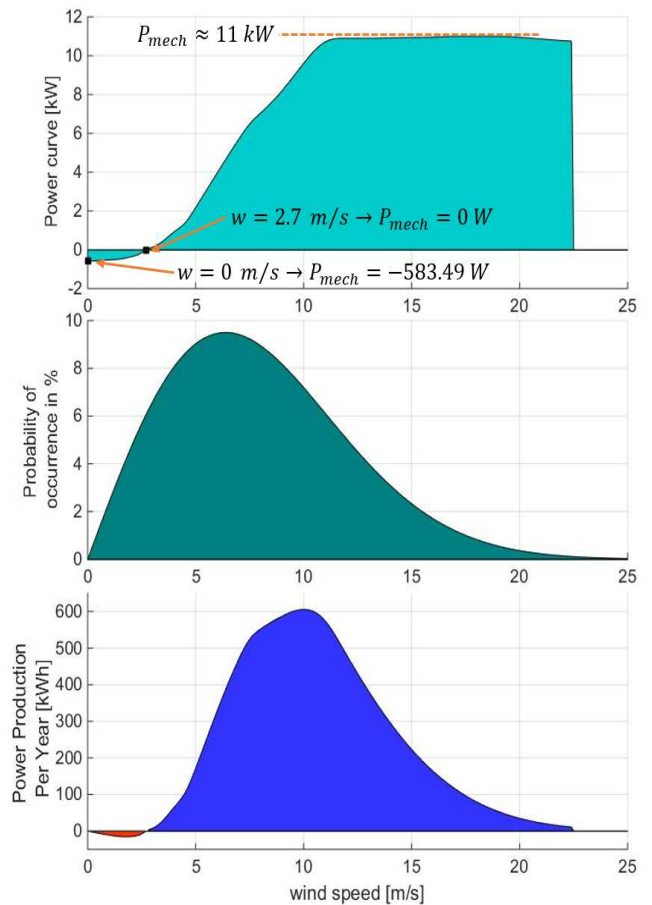


Fig. 10. From the top: power curve related to the *Pumping mode* AWES; Weibull probability density function for wind class 2; Power production per year where the orange area indicates the total energy used, while blue area stand for the total positive energy harvested.

V. CONCLUSIONS

In this paper we have shown that tether drag in an *Pumping mode* AWES plays an important role on the overall behavior. In particular, the amount of power produced is strongly downsized due the additional drag. A trend of minimum power consumption holding patterns which approach zero wind speed have been computed. By means of statistical analysis, it has been shown that the choice to continue flying during low wind conditions can potentially avoid the need for launch and landing procedures compared to a negligible amount of energy used to keep the aircraft airborne. These results have brought to light that AWE systems are sensitive to the tether effect and they suggest to spend more effort on the tether modeling with proper drag, e.g. model the tether as a set of point masses connected by inelastic rods [29], [30]. However may present some challenges if used in the context of controllers designed using predictive control algorithms.

VI. APPENDIX A

The aerodynamic forces and torques \bar{F} , \bar{M} are modeled using a standard coefficient approach plus an additional term coming from the approximation of the tether drag derived in section II. Let $\bar{v} = [v_x, v_y, v_z]^T$ the aircraft velocity relative to the wind \bar{w} in the reference frame \mathbf{e} given by

$$\bar{v} = \hat{r} - \bar{w}$$

defining the local unit vector in y direction as $\bar{e}_y = [0, 1, 0]^T$ and the $\hat{v} = \frac{\bar{v}}{\|\bar{v}\|}$ with $\|\bar{v}\|$ the euclidean norm of \bar{v} then the forces and moment can be written in a compact form as follow

$$\bar{F} = \frac{1}{2} \rho \|\bar{v}\|^2 S \mathbf{R} (C_L \bar{e}_y \times \hat{v} - C_D \hat{v} - C_Y (\bar{e}_y \times \hat{v}) \times \hat{v})$$

$$\bar{M} = \frac{1}{2} \rho S \|\bar{v}\|^2 [b C_l \quad c C_m \quad b C_n]^T$$

where ρ is the air density, b , c and S are respectively span, chord and wing area reference of the aircraft with \mathbf{R} the rotation matrix. Aerodynamic coefficient of lift C_L , drag C_D , side force C_Y , roll C_l , pitch C_m , yaw C_n . Defining the angle of attack α and sideslip angle β as

$$\alpha = \arctan\left(\frac{v_z}{v_x}\right) \quad \beta = \arcsin\left(\frac{v_y}{\|\bar{v}\|}\right)$$

the force coefficients are expressed as

$$\begin{aligned} \begin{bmatrix} C_L \\ C_D \\ C_Y \end{bmatrix} &= \begin{bmatrix} C_{L_0} + C_{L\alpha} \alpha \\ C_{D_0} + C_{D\alpha} \alpha + C_{D\alpha_2} \alpha^2 \\ C_{Y\beta} \beta \end{bmatrix} \\ &+ \begin{bmatrix} C_{L_e} \phi_e \\ C_{D_e} \phi_e + C_{D_{e_2}} \phi_e^2 + C_{D_{ae}} \alpha \phi_e \\ 0 \end{bmatrix} \\ &+ \begin{bmatrix} 0 \\ C_{D_a} \phi_a + C_{D_{a_2}} \phi_a^2 + C_{D_{\beta a}} \beta \phi_a \\ 0 \end{bmatrix} \\ &+ \begin{bmatrix} 0 \\ C_{D_{r_2}} \phi_r^2 + C_{D_{\beta r}} \beta \phi_r \\ C_{Y_r} \phi_r \end{bmatrix} + \begin{bmatrix} 0 \\ \frac{C_{D_N} d}{4S} l \\ 0 \end{bmatrix} \end{aligned}$$

as well as the moment coefficients

$$\begin{aligned} \begin{bmatrix} C_l \\ C_m \\ C_n \end{bmatrix} &= \begin{bmatrix} 0 \\ C_{m_0} \\ 0 \end{bmatrix} + \begin{bmatrix} C_{l\phi_a} & 0 & C_{l\phi_r} \\ C_{m\phi_a} & C_{m\phi_e} & C_{m\phi_r} \\ C_{n\phi_a} & 0 & C_{n\phi_r} \end{bmatrix} \begin{bmatrix} \phi_a \\ \phi_e \\ \phi_r \end{bmatrix} \\ &+ \frac{1}{2\|\bar{v}\|} \begin{bmatrix} C_{l_p} & C_{l_q} & C_{l_r} \\ C_{m_p} & C_{m_q} & C_{m_r} \\ C_{n_p} & C_{n_q} & C_{n_r} \end{bmatrix} \begin{bmatrix} b p \\ c q \\ b r \end{bmatrix} \\ &+ \begin{bmatrix} 0 & C_{l\beta} & C_{l\alpha\beta} \\ C_{m\alpha} & 0 & 0 \\ 0 & C_{n\beta} & C_{n\alpha\beta} \end{bmatrix} \begin{bmatrix} \alpha \\ \beta \\ \alpha\beta \end{bmatrix} \end{aligned}$$

TABLE I
MODEL PARAMETERS

Name	Symbol	Value
aircraft mass	m_a	36.8 kg
tether mass	m_t	1.5 kg
reference wing area	S	3 m ²
reference span	b	5.5 m
reference chord	c	0.55 m
moments of inertia	J_x, J_y, J_z	22, 32, 53 kg·m ²
radius winch	r_{winch}	0.25 m
cable thickness	d	0.002 m
drag coefficient	C_{D_N}	1.2
reference altitude	h_0	100 m
minimum altitude	h_{min}	100 m
roughness length	h_r	0.1 m
gravitational constant	g	9.81 m/s ²
air density	ρ	1.23 kg/m ³

TABLE II
TABLE OF CONSTRAINTS

Name	Unit	Bounds
tether length	m	$1 \leq l \leq 1000$
tether speed	m/s	$-9.5 \leq \dot{l} \leq 9.5$
tether acceleration	m/s^2	$-15 \leq \ddot{l} \leq 15$
torque	$N \cdot m$	$\tau_{winch} \leq 500$
angle of attack	deg	$-8 \leq \alpha \leq 22$
sideslip angle	deg	$-5 \leq \beta \leq 5$
aileron deflection	deg	$-20 \leq \phi_a \leq 20$
elevator deflection	deg	$-30 \leq \phi_e \leq 30$
rudder deflection	deg	$-30 \leq \phi_r \leq 30$
deflection rate	rad/s	$-2 \leq \dot{\phi}_{a,e,r} \leq 2$

REFERENCES

- [1] M. Diehl: "Airborne Wind Energy: Basic Concepts and Physical Foundations", in Airborne Wind Energy. New York, NY, USA: Springer, 2013, pp. 3-22
- [2] R. Ruitkamp, S. Sieberling: "Description and Preliminary Test Results of a Six Degrees of Freedom Rigid Wing Pumping System", in Airborne Wind Energy. New York, NY, USA: Springer, 2013, pp. 443-458
- [3] D.V. Lind, "Analysis and Flight Test Validation of High Performance Airborne Wind Turbines", in Airborne Wind Energy. New York, NY, USA: Springer, 2013, pp. 473-490
- [4] M.L. Loyd: Crosswind Kite Power. Journal of Energy, 4(3):106-111, July 1980
- [5] J. F. Manwell, J. G McGowan, A. L. Rogers: Wind Energy Explained: Theory, Design and Application, Second Edition. John Wiley & Sons, Ltd, Chichester, UK, 2009

- [6] J. Andersson, J. Åkesson, M. Diehl: CasADi: A symbolic package for automatic differentiation and optimal control. In: Forth, S., Hovland, P., Phipps, E., Utke, J., Walther, A. (eds.) *Recent Advances in Algorithmic Differentiation*, Vol. 87, Lecture Notes in Computational Science and Engineering, pp. 297307. Springer, Berlin (2012). doi: 10.1007/978-3-642-30023-3_27
- [7] G. Horn: the RAWESOME Airborne Wind Energy Simulation, Optimization and Modeling Environment, <https://github.com/ghorn/rawesome>
- [8] A. Wächter, L. Biegler: On the Implementation of a Primal-Dual Interior Point Filter Line Search Algorithm for Large-Scale Nonlinear Programming. *Mathematical Programming* 106(1), 2557 (2006). doi: 10.1007/s10107-004-0559-y
- [9] B. Houska, M. Diehl: Optimal control of towing kites. In: *Proceedings of the 45th IEEE Conference on Decision and Control*, pp. 26932697, San Diego, CA, USA, 1315 Dec 2006. doi: 10.1109/CDC.2006.377210
- [10] I. Argatov, R. Silvennoinen: Energy conversion efficiency of the pumping kite wind generator. *Renewable Energy* 35(5), 10521060 (2010). doi: 10.1016/j.renene.2009.09.006
- [11] S. Sieberling, R. Ruiterkamp, The PowerPlane an Airborne Wind Energy System - Conceptual Operations, 11th AIAA Aviation Technology, Integration, and Operations (ATIO) Conference
- [12] G. Horn, S. Gros, M. Diehl: "Numerical Trajectory Optimization for Airborne Wind Energy Systems Described by High Fidelity Aircraft Models", in *Airborne Wind Energy*. New York, NY, USA: Springer, 2013, pp. 205-218
- [13] J. Stuyts, G. Horn, W. Vandermeulen, J. Driesen, M. Diehl: Effect of the Electrical Energy Conversion on Optimal Cycles for Pumping Airborne Wind Energy, *IEEE Trans. Sustainable Energy*, vol. 6, pp. 2-10, Sep 2014. DOI:10.1109/TSTE.2014.2349071
- [14] S. Gros, M. Diehl: "Modeling of Airborne Wind Energy Systems in Natural Coordinates", in *Airborne Wind Energy*. New York, NY, USA: Springer, 2013, pp. 181-202
- [15] S. Gros, M. Diehl: A Relaxation Strategy for the Optimization of Airborne Wind Energy Systems. In: *Proceedings of the European Control Conference (ECC13)*, Zurich, Switzerland, 1719 July 2013
- [16] U. M. Ascher, L. R. Petzold: *Computer Methods for Ordinary Differential Equations and Differential Algebraic Equations*. SIAM Press, Philadelphia (1998)
- [17] S. Gros, M. Zanon, M. Vukov, M. Diehl: Nonlinear MPC and MHE for Mechanical Multi-Body Systems with Application to Fast Tethered Airplanes. In: *Proceedings of the 4th IFAC Nonlinear Model Predictive Control Conference*, pp. 8693, Leeuwenhorst, Netherlands, 2327 Aug 2012. doi: 10.3182/20120823-5-NL-3013.00061
- [18] L.T. Biegler. *Nonlinear Programming*. 2010
- [19] A. A. Shabana: *Dynamics of Multibody Systems*. 3rd ed. Cambridge University Press, Cambridge (2005)
- [20] I. Troen, E.L. Petersen: *European Wind Atlas*. Risoe National Laboratory, Risoe, Denmark, 1991
- [21] B. Houska, M. Diehl: Optimal Control for Power Generating Kites. Proc. 9th European Control Conference (2007)
- [22] S. Kameswaran, L. Biegler: Simultaneous dynamic optimization strategies: Recent advances and challenges. *Computers and Chemical Engineering* 30(1112), 15601575 (2006). doi: 10.1016/j.compchemeng.2006.05.034
- [23] K. Geebelen, M. Vukov, A. Wagner, H. Ahmad, M. Zanon, S. Gros, D. Vandepitte, J. Swevers, M. Diehl: "An Experimental Test Setup for Advanced Estimation and Control of an Airborne Wind Energy System", in *Airborne Wind Energy*. New York, NY, USA: Springer, 2013, pp. 459-471
- [24] C. L. Archer: "An Introduction to Meteorology for Airborne Wind Energy", in *Airborne Wind Energy*. New York, NY, USA: Springer, 2013, pp. 81-94
- [25] M. Zanon, S. Gros, M. Diehl: "Model Predictive Control of Rigid-Airfoil Airborne Wind Energy Systems", in *Airborne Wind Energy*. New York, NY, USA: Springer, 2013, pp. 219-223
- [26] J. Nocedal, S.J. Wright: *Numerical Optimization*. Springer Series in Operations Research and Financial Engineering. Springer, 2 edition, 2006
- [27] Ampyx Power: Airborne Wind Energy [Online]. Available: <https://www.ampyxpower.com/>
- [28] J.F. Manwell, J.G. McGowan, A.L. Rogers: "Wind Characteristics and Resources", in *Wind Energy Explained - Theory, Design and Application*. Amherst, USA: Wiley, 2002, pp. 21-82
- [29] P. Williams, B. Lansdorp, W.J. Ockels: Modeling and Control of a Kite on a Variable Length Flexible Inelastic Tether. AIAA Paper 2007-6705. In: *Proceedings of the AIAA Modelling and Simulation Technologies Conference and Exhibit*, Hilton Head, SC, USA, 2023 Aug 2007. doi: 10.2514/6.2007-6705
- [30] P. Williams, B. Lansdorp, W. Ockels: Optimal Crosswind Towing and Power Generation with Tethered Kites. *AIAA Journal of Guidance, Control, and Dynamics* 31(1), 8193 (2008). doi: 10.2514/1.30089
- [31] J. Gillis, J. Goos, K. Geebelen, J. Swevers, M. Diehl: Optimal periodic control of power harvesting tethered airplanes: how to fly fast without wind and without propeller?. *American Control Conference*, Montreal, QC, 27-29 June 2012. DOI: 10.1109/ACC.2012.6314924